



Article

# Spatiotemporal Analysis of Black Carbon Sources: Case of Santiago, Chile, under SARS-CoV-2 Lockdowns

Carla Adasme <sup>1,2</sup>, Ana María Villalobos <sup>1</sup> and Héctor Jorquera <sup>1,2,\*</sup> 

<sup>1</sup> Departamento de Ingeniería Química y Bioprocesos, Pontificia Universidad Católica de Chile, Santiago 7820436, Chile

<sup>2</sup> Centro de Desarrollo Urbano Sustentable (CEDEUS), Los Navegantes 1963, Providencia, Santiago 7520246, Chile

\* Correspondence: jorquera@ing.puc.cl; Tel.: +56-95504-4421

**Abstract:** Background: The SARS-CoV-2 pandemic has temporarily decreased black carbon emissions worldwide. The use of multi-wavelength aethalometers provides a quantitative apportionment of black carbon (BC) from fossil fuels ( $BC_{ff}$ ) and wood-burning sources ( $BC_{wb}$ ). However, this apportionment is aggregated: local and non-local BC sources are lumped together in the aethalometer results. Methods: We propose a spatiotemporal analysis of BC results along with meteorological data, using a fuzzy clustering approach, to resolve local and non-local BC contributions. We apply this methodology to BC measurements taken at an urban site in Santiago, Chile, from March through December 2020, including lockdown periods of different intensities. Results:  $BC_{ff}$  accounts for 85% of total BC; there was up to an 80% reduction in total BC during the most restrictive lockdowns (April–June); the reduction was 40–50% in periods with less restrictive lockdowns. The new methodology can apportion  $BC_{ff}$  and  $BC_{wb}$  into local and non-local contributions; local traffic (wood burning) sources account for 66% (86%) of  $BC_{ff}$  ( $BC_{wb}$ ). Conclusions: The intensive lockdowns brought down ambient BC across the city. The proposed fuzzy clustering methodology can resolve local and non-local contributions to BC in urban zones.

**Keywords:** black carbon; aethalometer model; spatiotemporal patterns; fuzzy clustering; FUSTA



**Citation:** Adasme, C.; Villalobos, A.M.; Jorquera, H. Spatiotemporal Analysis of Black Carbon Sources: Case of Santiago, Chile, under SARS-CoV-2 Lockdowns. *Int. J. Environ. Res. Public Health* **2022**, *19*, 17064. <https://doi.org/10.3390/ijerph192417064>

Academic Editors: Isidro A. Pérez and M. Ángeles García

Received: 15 November 2022

Accepted: 13 December 2022

Published: 19 December 2022

**Publisher's Note:** MDPI stays neutral with regard to jurisdictional claims in published maps and institutional affiliations.



**Copyright:** © 2022 by the authors. Licensee MDPI, Basel, Switzerland. This article is an open access article distributed under the terms and conditions of the Creative Commons Attribution (CC BY) license (<https://creativecommons.org/licenses/by/4.0/>).

## 1. Introduction

Black carbon (BC) is one of the components of fine respirable particle matter ( $PM_{2.5}$ ); it comes from the incomplete combustion of fossil fuels and biomass. Exposure to BC has been linked to short-term [1,2] and long-term [3–7] health effects, but its regulation is indirect through the regulation of ambient  $PM_{2.5}$ . Recently, the World Health Organization has updated its air quality guidelines [8], setting an annual average of  $PM_{2.5}$  of  $5 \mu\text{g}/\text{m}^3$ , which means that long-term BC is implicitly recommended to be well below that guideline since BC is usually below 20% of the total  $PM_{2.5}$ .

BC has been traditionally measured offline using thermal-optical methods applied to filter samples [9,10]; these results are reported as total BC in  $PM_{2.5}$  [11]. More recently, continuous instruments based on optical absorption at several wavelengths (from UV to IR) have been developed. These instruments (aethalometers) can apportion BC coming from fossil fuel ( $BC_{ff}$ ) and wood burning ( $BC_{wb}$ ) combustion because the BC emitted from those sources has a different wavelength dependence for that absorption [12]. This technological development has led to many studies worldwide that report that BC source apportionment in urban [13–20] and rural areas [21–23]. Despite this improvement, those apportionment results—on any given receptor site—report the total  $BC_{ff}$  (or  $BC_{wb}$ ) coming from local and non-local sources; for instance, regional wildfires may contribute to  $BC_{wb}$  as much as local sources,  $BC_{ff}$  may come from local and regional traffic sources, etc. Additional tools, like air quality models, have been used to resolve those local and non-local BC contributions [24]. Recently, aethalometers have been used to assess the changes in ambient  $BC_{ff}$  and  $BC_{wb}$

associated with urban lockdowns worldwide [25–31]. All these studies report significant decreases in ambient BC concentrations under those exceptional circumstances, with traffic sources being the largest contributors to those decreases, while  $BC_{wb}$  sometimes has not changed [29] or has even increased [32].

The purpose of this work is twofold: (a) report ambient  $BC_{ff}$  and  $BC_{wb}$  concentrations for the very first time in Santiago, Chile, and estimate the reductions in ambient BC concentrations brought by lockdowns during SARS-CoV-2 pandemics, (b) apply a new methodology of spatiotemporal pattern recognition for estimating local and non-local contributions to ambient  $BC_{ff}$  and  $BC_{wb}$ .

The new methodology is based on a fuzzy clustering algorithm applied to ambient  $BC_{ff}$  and  $BC_{wb}$  concentrations along with surface meteorological variables (wind speed and direction, air temperature). This methodology—named FUSTA (Fuzzy SpatioTemporal Apportionment)—splits ambient concentrations into several spatiotemporal patterns, each one corresponding to a contribution from one of the major emission sources [32]. This novel method generates a source apportionment for local and non-local BC sources without the need for air quality modeling applied to the city. The latter would require (a) an accurate emission inventory for  $BC_{ff}$  and  $BC_{wb}$ , (b) the meteorological input fields should be accurate and capture the strong mixing layer seasonality over Santiago, and (c) the air quality model used should not have significant biases.

We find a reduction in total BC in Santiago during the lockdowns in 2020, from 40% to 80%, as compared with previous measurements in 2015; we also find that the FUSTA approach is a useful tool to resolve local and non-local sources of  $BC_{ff}$  and  $BC_{wb}$ .

## 2. Materials and Methods

The methodology follows a sequential process, as shown in Figure 1. Below, we describe each of the methodological steps.

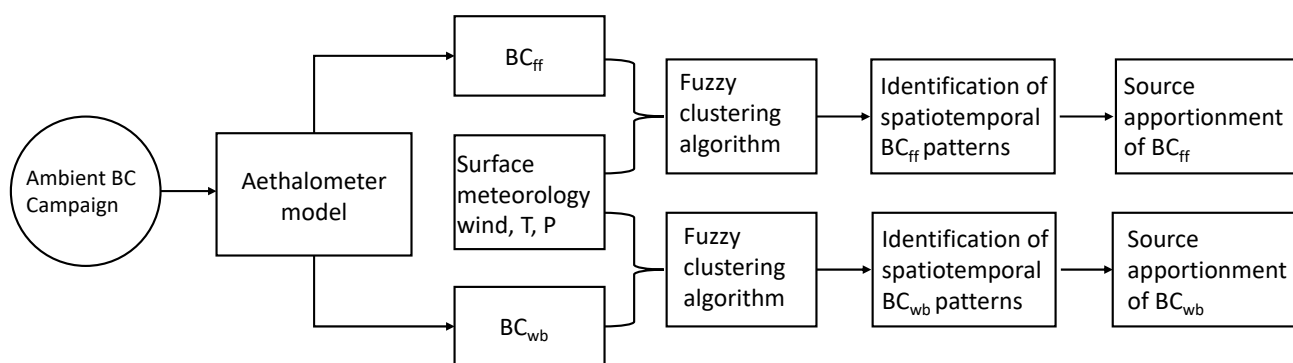


**Figure 1.** Workflow of the methodology.

### 2.1. Ambient Measurement Campaign

The measurement campaign was carried out between 16 March 2020 and 2 January 2021. Lockdowns started on 27 March in the NE part of the city, and on 23 April, the SW sector of the city was added. Later on 15 May, a total lockdown was enacted until 27 July, followed by less restrictive lockdowns in the city until 30 November, when another rise in people infected forced the government to increase mobility restrictions again [33].

The monitoring was conducted using a multiwavelength aethalometer (MA200, San Francisco, CA, USA) measuring at five wavelengths: 375, 470, 538, 625, and 880 nm, corresponding to ultraviolet, blue, green, red and infrared, respectively. The monitoring site was chosen in a residential area located on the east border of the city (33.406° S, 70.512° W). Surface meteorological data were taken from a nearby site (33.377° S, 70.523° W), which corresponds to an air quality station (Las Condes) run by the Ministry of the Environment [34]. The location of the monitoring site was chosen on the east border of the city to capture the city's pollution plume arriving at that site when daylight anabatic winds develop. That

zone of the city has been studied before with ambient BC campaigns [24], so there was a baseline available to make comparisons with/without lockdowns.

The total BC signal recorded from the instrument was calibrated against the thermal optical transmittance method (TOT) NIOSH 5050 results applied to co-located PM<sub>2.5</sub> samples taken on 47 mm quartz filters (Pallflex Tissuquartz 2500QAT-UP, Pall Life Sciences, Portsmouth, UK) using a minivol sampler (Super SASS, MetOne Instruments, Grants Pass, OR, USA); the BC TOT analysis was carried out at Chester LabNet (Tigard, OR, USA).

## 2.2. Aethalometer Data Analysis

Hourly averages of absorption coefficients ( $b_{\text{abs}}$ ) measured at 375 and 880 nm reported by the MA200 are used to compute the Absorption Ångström Exponent (AAE) according to [12]:

$$\text{AAE} = -\ln(b_{\text{abs}}(375 \text{ nm})/b_{\text{abs}}(880 \text{ nm}))/\ln(375/880) \quad (1)$$

The histogram of hourly values of AAE is analyzed, and the 1st and 99th percentiles are identified with the Ångström exponents for fossil fuel ( $\text{AAE}_{\text{ff}}$ ) and wood burning ( $\text{AAE}_{\text{wb}}$ ), respectively [35]; the estimated values are  $\text{AAE}_{\text{ff}} = 0.7$  and  $\text{AAE}_{\text{wb}} = 2.48$ . Appendix A shows how this estimation was carried out.

Next, the contributions  $\text{BC}_{\text{ff}}$  and  $\text{BC}_{\text{wb}}$  are computed as [12]:

$$\text{BC}_{\text{ff}} = \text{BC}_{\text{total}} \cdot b_{\text{abs,ff}}(880 \text{ nm})/b_{\text{abs}}(880 \text{ nm}) \quad (2)$$

$$\text{BC}_{\text{wb}} = \text{BC}_{\text{total}} \cdot b_{\text{abs,wb}}(880 \text{ nm})/b_{\text{abs}}(880 \text{ nm}) \quad (3)$$

where  $\text{BC}_{\text{total}}$  is the total BC reading of the instrument at 880 nm, and the following expressions are used to estimate the absorption coefficients  $b_{\text{abs,ff}}$  and  $b_{\text{abs,wb}}$  [12]:

$$b_{\text{abs,ff}}(880 \text{ nm}) = \{b_{\text{abs}}(375 \text{ nm}) - b_{\text{abs}}(880 \text{ nm}) \cdot (375/880)^{-\text{AAE}_{\text{ff}}}\} / \{(375/880)^{-\text{AAE}_{\text{wb}}} - (375/880)^{-\text{AAE}_{\text{ff}}}\} \quad (4)$$

$$b_{\text{abs,wb}}(880 \text{ nm}) = \{b_{\text{abs}}(375 \text{ nm}) - b_{\text{abs}}(880 \text{ nm}) \cdot (375/880)^{-\text{AAE}_{\text{wb}}}\} / \{(375/880)^{-\text{AAE}_{\text{ff}}} - (375/880)^{-\text{AAE}_{\text{wb}}}\} \quad (5)$$

## 2.3. Spatiotemporal Data Analysis

In a previous publication [36], we used bivariate plots and k-means clustering of ambient PM<sub>2.5</sub> and PM<sub>10</sub>, along with receptor model results, to estimate major sources contributing to ambient PM in urban areas; this methodology works best when one or two sources are the major contributors to ambient concentrations. However, this approach has two limitations: (i) the bivariate plots accept only pairs of meteorological variables to analyze ambient PM concentrations, (ii) the clustering technique is hard, that is, each hourly observation may belong to only one cluster (source). To improve the flexibility of that analysis, the meteorological input variables were increased to four: wind speed, wind direction, temperature, and pressure. But the key improvement is to use a fuzzy clustering algorithm, so each hourly observation may belong to more than one (fuzzy) cluster, using the probabilistic concept of cluster membership [37]. The proof of the concept of this new approach (denoted as FUSTA: FUZZY SpatioTemporal Apportionment) was developed for ambient SO<sub>2</sub> in an industrial zone, where it was shown that spatiotemporal patterns obtained from FUSTA were like the ones obtained by air quality modeling of the major SO<sub>2</sub> emission sources in the study zone [32]. This was the rationale for hypothesizing that FUSTA could resolve local and non-local sources of  $\text{BC}_{\text{ff}}$  and  $\text{BC}_{\text{wb}}$  because these are inert tracers of combustion sources, so they are only subject to atmospheric transport and deposition. Below we summarize the major steps needed to carry out such a methodology for the case of black carbon.

Data of  $\text{BC}_{\text{ff}}$  and  $\text{BC}_{\text{wb}}$  are log transformed to approach a normal distribution. Each of them is combined with air temperature and pressure and the Cartesian components of wind speed as in the case of bivariate plots [38]. These 5D databases are analyzed to find spatiotemporal patterns in  $\text{BC}_{\text{ff}}$  and  $\text{BC}_{\text{wb}}$  by using the algorithm FKM.ent.noise [39] available in the library fclust in the R environment [40]. The following optimization is

carried out to find the centroids {C} and membership values  $U = \{u_{ij}\}$  for the case of  $p$  fuzzy clusters sought:

$$\begin{aligned} \min_{U,C} J_{FKMNE} &= \sum_{i=1}^n \sum_{k=1}^p u_{ik} \cdot \|x_i - c_k\|^2 + t \cdot \sum_{i=1}^n \sum_{k=1}^p u_{ik} \cdot \log(u_{ik}) + \sum_{i=1}^n \delta^2 \left(1 - \sum_{k=1}^p u_{ik}\right)^2 \\ \text{s.t. } u_{ik} &\in [0, 1]; \sum_{k=1}^{p+1} u_{ik} = 1 \end{aligned} \tag{6}$$

where we use the default values  $t = 1$  and  $\delta = 1$  in the above equation [39]. The very last term on the right-hand side of (6) stands for a noise cluster, that is, a subset of data that does not follow a regular pattern as the other  $p$  fuzzy clusters do [41]. This noise cluster includes outlier values or contributions from intermittent sources like a structural fire or a wildfire plume reaching the monitoring site, for instance.

Once the solution of (6) is found, the  $BC_{ff}$  estimated at time ‘ $i$ ’ from Equations (2) and (4) is apportioned as follows:

$$BC_{ffi} = \sum_{k=1}^{p+1} BC_{ffi} \cdot u_{ik} = \sum_{k=1}^p BC_{ffi,k} + BC_{ffi,noise} \tag{7}$$

where  $BC_{ffi,k}$  stands for the contribution of the  $k$ -th cluster (or source) to  $BC_{ffi}$ . A similar equation holds for  $BC_{wbi}$ . Note that, by design, all those contributions are non-negative.

Since the results are 5D objects, we project the resulting fuzzy clusters using 3 different bivariate plots [38,42,43] in which wind direction is combined with wind speed, temperature, and pressure, respectively, to visualize the spatial distribution of fuzzy clusters found for each BC fraction. These graphs support the task of identifying each of the fuzzy clusters resolved by the FUSTA algorithm (6).

The database and all routines used in the data analysis and visualization are provided as Supplementary Files.

### 3. Results

#### 3.1. Ambient Monitoring Results

##### 3.1.1. Absorption Ångström Exponents (AAE)

The following table lists the statistics for the estimated absorption Ångström exponents and estimated concentrations of  $BC_{ff}$ ,  $BC_{wb}$  and  $BC$  for the whole campaign.

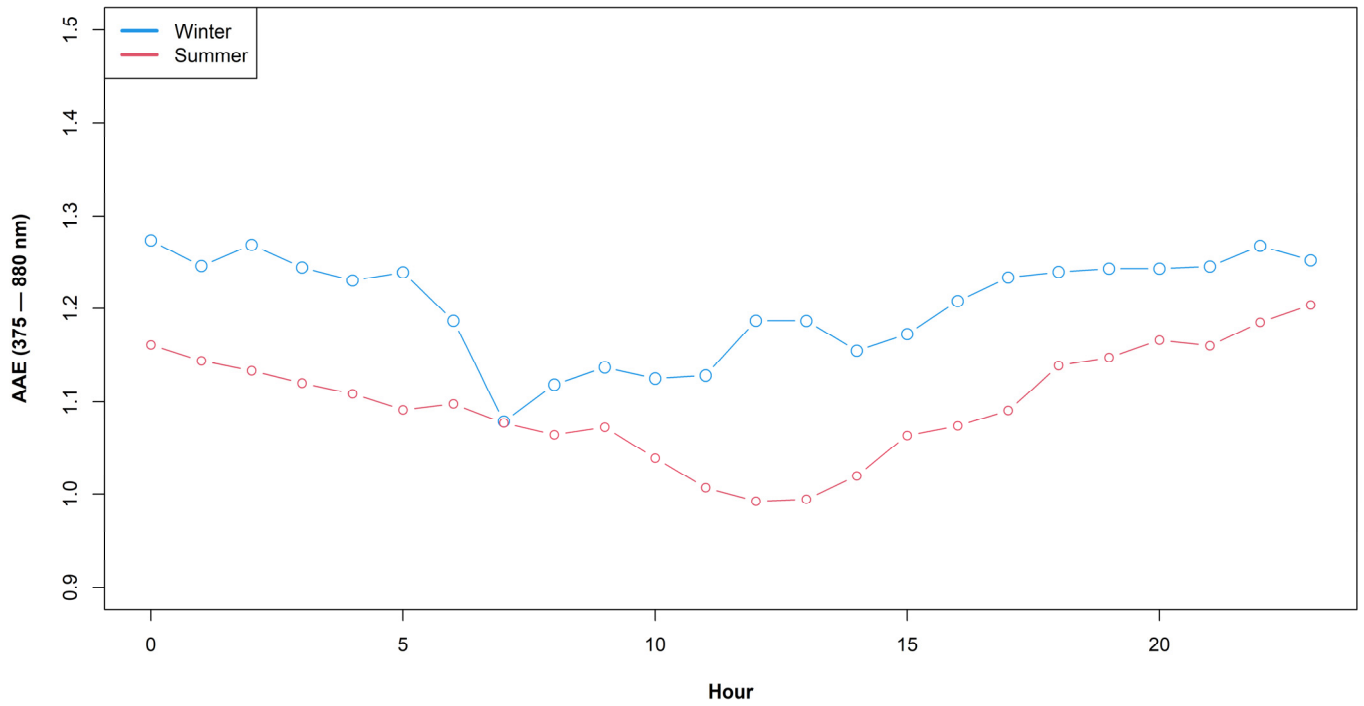
Figure 2 shows the diel profiles of AAE for the austral summer and winter months. The winter mean value is significantly higher than the summer value ( $t = 11.9$ ,  $p$ -value  $< 2.2 \times 10^{-16}$ ), which suggests that wood-burning contributions to AAE increase in winter because of residential space heating in the city, a well-known source of ambient  $PM_{2.5}$  in Santiago [44].

Figure 3 shows a comparison of diel profiles of AAE for workdays and weekends. During weekends, the AAE mean value is significantly higher than in the case of workdays ( $t = 7.64$ ,  $p$ -value  $= 2.8 \times 10^{-14}$ ); this suggests a higher consumption of wood burning on weekends and thus the increase in AAE values.

##### 3.1.2. $BC_{ff}$ and $BC_{wb}$ Results

Figure 4 shows the time variability for  $BC_{ff}$  and  $BC_{wb}$  contributions estimated from the aethalometer model.  $BC_{ff}$  is the dominant contribution to total BC all year long; this contribution decreases over weekends, as expected from the traffic activity variability in the city. From Table 1, it follows that, on average,  $BC_{ff}$  accounts for 85% of total BC. Regarding  $BC_{wb}$  contribution (see Figure A3), it rises in winter months, as expected, and it does not decrease over weekends since it comes from residential sources. This contribution does not vanish in the spring and summer seasons; this is explained by wildfires and agricultural burning sources at the regional scale; they have been found in Santiago using receptor modeling of ambient  $PM_{2.5}$  combined with satellite images [45].

**Diel variation AAE**



**Figure 2.** Diel profiles of AAE for (austral) summer and winter months.

**Diel variation AAE**

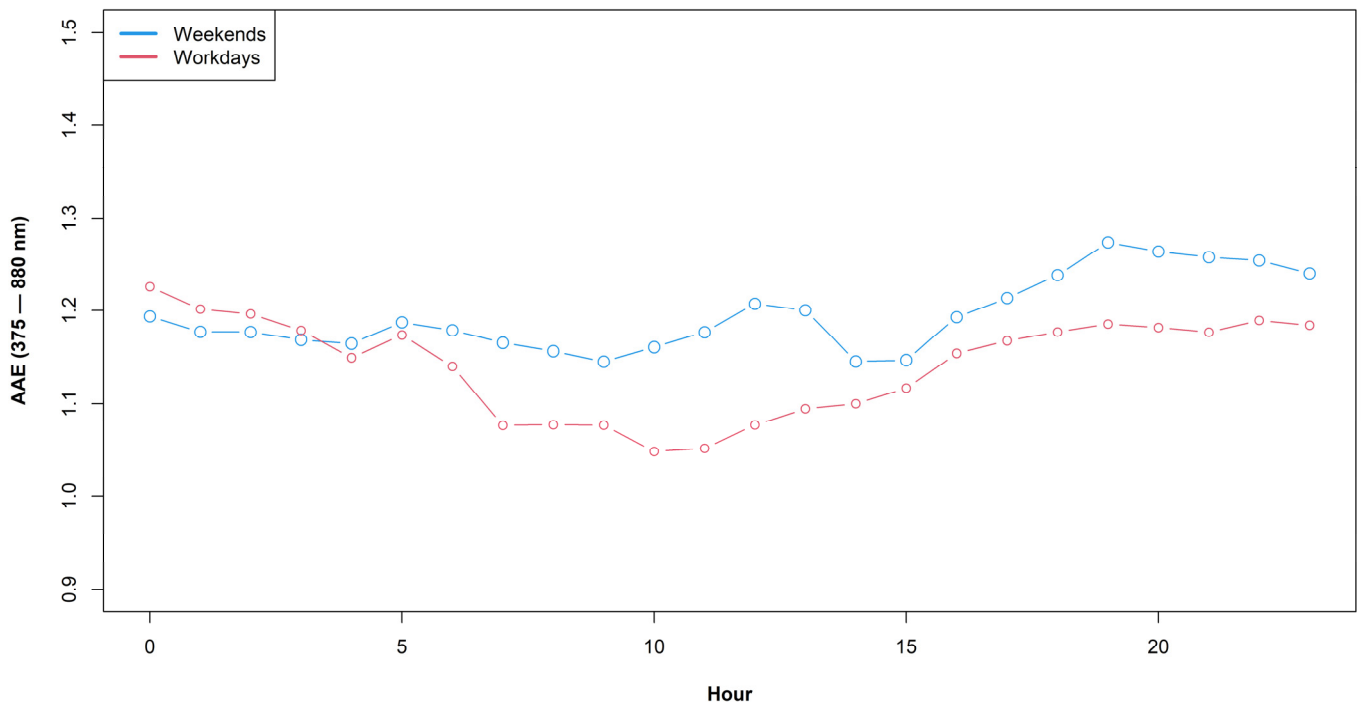


**Figure 3.** Diel profiles of AAE for workdays and weekends.

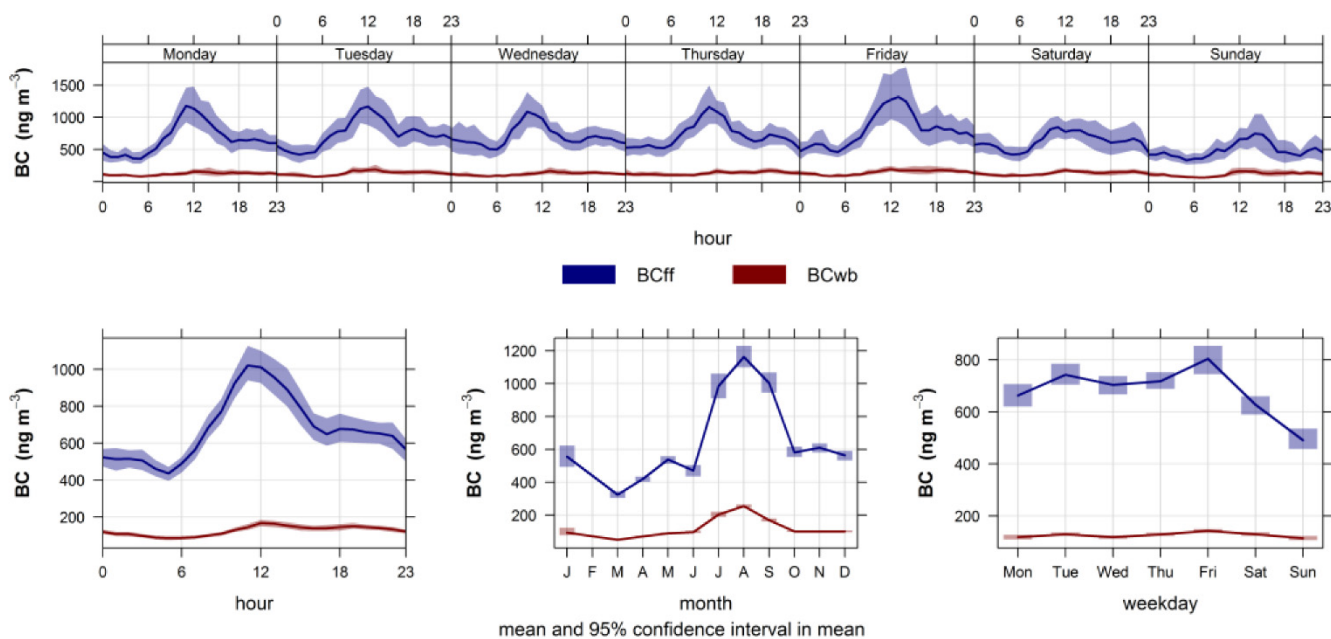


Figure 4. Time variability plot for  $BC_{ff}$  and  $BC_{wb}$  contributions.

Table 1. Statistical summary of campaign results <sup>1</sup>.

Statistic	AAE (-)	$BC_{ff}$ (ng/m <sup>3</sup> )	$BC_{wb}$ (ng/m <sup>3</sup> )	BC (ng/m <sup>3</sup> )
Minimum	0.002	0.62	0.04	0.11
1st quantile	1.036	294	55	357
Median	1.135	488	90	585
Mean	1.160	690	128	809
3rd quartile	1.237	847	156	988
Maximum	3.322	7812	1604	8679

<sup>1</sup> Negative values are excluded from the statistics (see also Appendix A).

### 3.1.3. Effect of SARS-CoV-2 Lockdowns on BC Concentrations

There is no continuous monitoring of ambient BC in Santiago. However, there was an ambient monitoring campaign that included BC measurements at nearby Las Condes station from December 2014 through July 2015, using an aethalometer (Magee Scientific, Berkeley, CA, USA, model AE33); that campaign results are reported in [24]. Table 2 below makes a comparison of monthly average BC values between that campaign and present results. The most intensive city lockdowns led up to an 80% of reduction in total BC (June 2020), and a 40% reduction has been estimated with fewer intensive lockdowns in December 2020 [33].

### 3.2. Spatiotemporal Analysis

The fuzzy clustering algorithm of Equation (6) was applied to both datasets of ambient  $BC_x$  and meteorology ( $x = ff$  or  $wb$ ), and the total number of clusters sought was varied between four and seven clusters— $p = 3-6$  in Equation (6), respectively. Then, we inspected the time variability of the resulting spatiotemporal patterns (i.e., fuzzy clusters). Based on the similarities in temporal and spatial variability, we identified the major sources contributing to ambient  $BC_x$  concentrations. Below we discuss the results for both BC components.

**Table 2.** Comparison of ambient BC measurements in east Santiago, monthly averages (ng/m<sup>3</sup>).

Month	2015 <sup>1</sup>	2020 <sup>3</sup>	Ratio 2020/2015
January	1200		
February	1063		
March	1583	376 ± 50	0.24
April	2233	495 ± 62	0.22
May	2440	627 ± 100	0.26
June	2877	533 ± 97	0.19
July	2430	1207 ± 279	0.50
August		1435 ± 196	
September		1137 ± 268	
October		682 ± 93	
November		706 ± 90	
December	1073 <sup>2</sup>	672 ± 68	0.63

<sup>1</sup> Data adapted from [24]. <sup>2</sup> Data correspond to December 2014. <sup>3</sup> Data reported as mean ± 2σ, estimated from daily averages with at least 75% of valid hourly values.

### 3.2.1. Results for BC<sub>ff</sub>

Upon inspection of the different FUSTA results for this BC fraction, the contributions from Santiago's urban plume arriving at the monitoring site and the noisy cluster contributions were identified by their distinctive upwind locations—W-SW and SSE, respectively (see Figures A4, A5 and 6, below). A residential heating and cooking contribution (RHC) was identified because it is highest overnight when temperatures are lowest—in the winter season. Then, the rest of the contributions are traffic sources located in different directions upwind of the monitoring site. Since the only contribution that vanishes in winter is Santiago's urban plume, we conclude that all other contributions are local, and they arrive at the monitoring site from different upwind directions and under different combinations of air temperature and pressure (Figures A4, A5 and 6). Table 3 summarizes the mean source contribution estimated in each case. A small variability in major source contribution estimates is observed in these results.

**Table 3.** Mean source contributions to BC<sub>ff</sub> (ng/m<sup>3</sup>) for a different choice of total clusters sought.

Total Clusters	Urban Plume	RHC	TRF	Other (Noise)
4	109	unresolved	505	80
5	98	90	458	48
6	91	78	486	40
7	87	54	528	27

Hence, for simplicity's sake, we chose the lowest number of fuzzy clusters (5) that apportion all major BC<sub>ff</sub> sources at play. Figures 5 and 6 display the temporal and spatial variability of those clusters, respectively, and Table 4 provides a statistical summary of cluster contributions; additional bivariate plots for BC<sub>ff</sub> are presented in Appendix B (Figures A4 and A5). Below we discuss the features of this five-cluster solution.

**Table 4.** Statistical summary of hourly BC<sub>ff</sub> source contributions (ng/m<sup>3</sup>) for a 5-cluster solution.

Statistic	Cluster 1	Cluster 2	Cluster 3	Cluster 4	Cluster 5
Minimum	0.0	0.0	0.0	0.0	0.15
1st quartile	0.0	5.2	4.5	0.7	0.63
Median	0.22	51.5	45.0	24.2	1.86
Mean	98.0	90.4	143	315	47.7
3rd quartile	17.4	150.8	215	313	9.4
Maximum	2313	641	1695	5304	6296

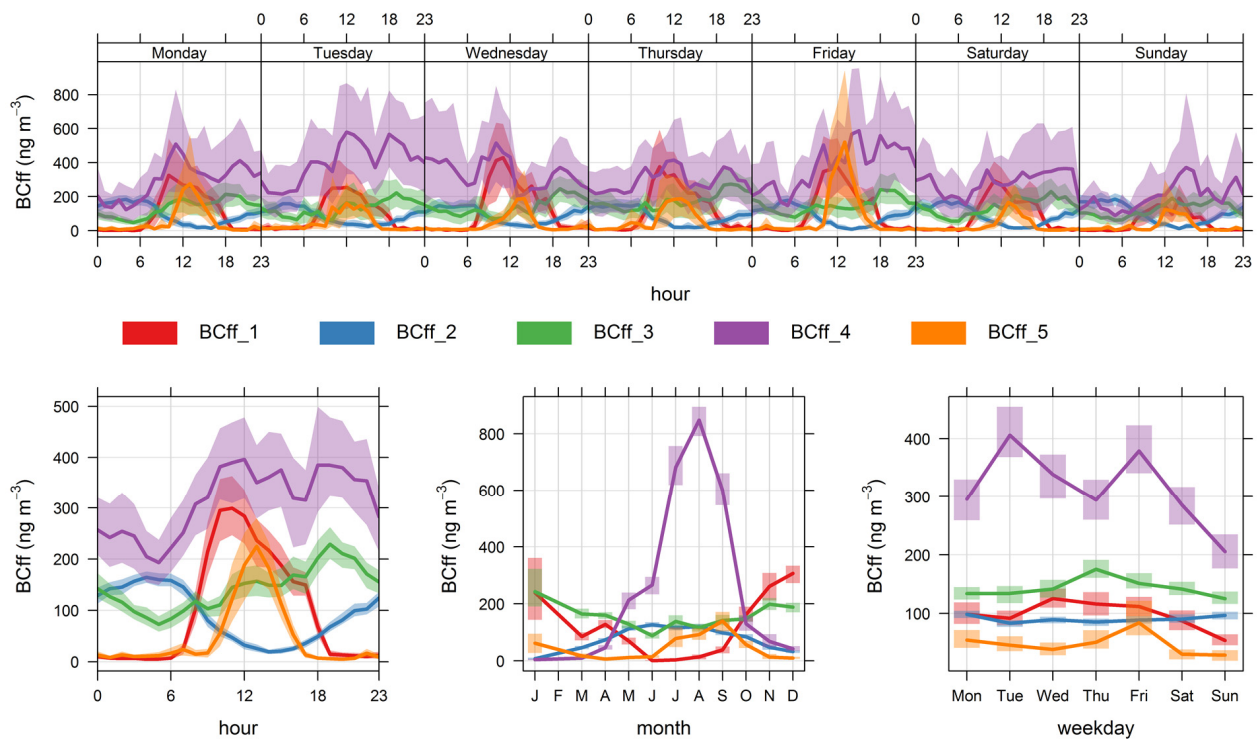


Figure 5. Time variability plot for the five fuzzy clusters' contributions to BC<sub>ff</sub>.

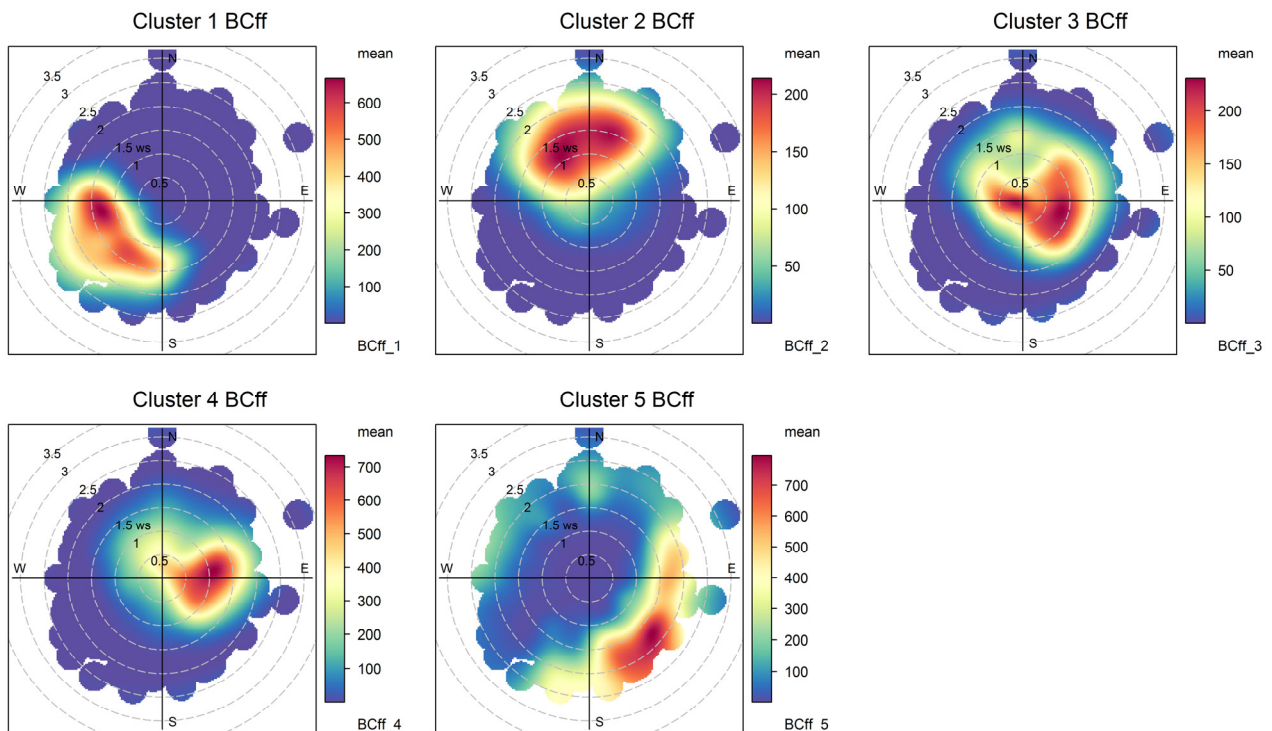


Figure 6. Bivariate plots for the five fuzzy clusters' contributions to BC<sub>ff</sub>.

Cluster 1 contributions rise in the daylight hours and are zero overnight; these contributions increase in the austral summer season and decrease over weekends. Since they come from W/SW directions, this fuzzy cluster is identified as Santiago's urban plume reaching the monitoring site as anabatic winds develop during daylight. Contributions of this source are highest when temperatures and wind speed increase in the summer season; this air quality feature of the eastern side of Santiago has been described before [36,46].

On average, this source contributes 14% of the total  $BC_{ff}$ . Notice that in Table 4, this contribution has more than 25% of hours with zero contribution, which corresponds to overnight conditions.

Cluster 2 contributions increase in the evening hours and reach a maximum before sunrise (when the mixing layer is lowest), are highest in the winter season and low temperatures (Figure A4); they arrive at the monitoring site from different directions (NW–NE) which agree with the highest population density surrounding this site. We identify this source contribution as residential heating and cooking (RHC) sources that use compressed natural gas and liquified petroleum gas as fuels. They contribute on average with 13% of total  $BC_{ff}$ .

Clusters 3 and 4 rise in the morning, peak in the evening, and decrease until dawn; since they also decrease over weekends, we identify those two clusters as local traffic (TRF) sources. Together they account for 66% of total  $BC_{ff}$ . These two clusters are resolved by the algorithm because they have different seasonality; cluster 4 contributions are higher when temperatures are lower and winds weaker, so this cluster has the highest seasonality of all.

Cluster 5 includes all sources whose spatiotemporal patterns are intermittent, so they are identified as local combustion sources that peak around 1 pm in winter, most likely associated with residential cooking and heating. On average, this source contributes the least to total  $BC_{ff}$ , with 7%.

### 3.2.2. Results for $BC_{wb}$

We applied the same criteria to identify the contributions of different FUSTA solutions for the  $BC_{wb}$  fraction. Thus, we identified Santiago’s urban plume and noise contributions by their distinctive upwind locations—W-SW and SSE, respectively (Figures A6, A7 and 8, below). Once again, only the urban plume contribution vanishes in the winter season—when a low thermal inversion layer blocks air masses from the lower valley from reaching the monitoring site—so the rest of the sources must be local ones. Table 5 shows the mean source contribution estimated for each source as the number of clusters increases. Again, a small variability in major source contribution estimates is observed in these results.

**Table 5.** Mean source contributions to  $BC_{wb}$  ( $ng/m^3$ ) for a different choice of total clusters sought.

Total Clusters	Urban Plume	Local Wood Burning	Other Local (Noise)
4	18	96	14
5	17	103	8
6	15	106	7
7	14	109	5

Again, for simplicity, we have chosen to present the results for four (total) clusters in this case. The results are shown below in Figures 7 and 8 and Table 6; additional bivariate plots for  $BC_{wb}$  are presented in Appendix B (Figures A6 and A7). Below we discuss the features of this four-cluster solution.

**Table 6.** Statistical summary of  $BC_{wb}$  source contributions ( $ng/m^3$ ).

Statistic	Cluster 1	Cluster 2	Cluster 3	Cluster 4
Minimum	0.00	0.0	0.00	0.04
1st quantile	0.34	2.37	0.00	0.24
Median	13.1	19.1	0.12	0.73
Mean	64.0	31.8	18.4	14.0
3rd quartile	82.6	49.7	7.9	4.1
Maximum	873	265	387	1506

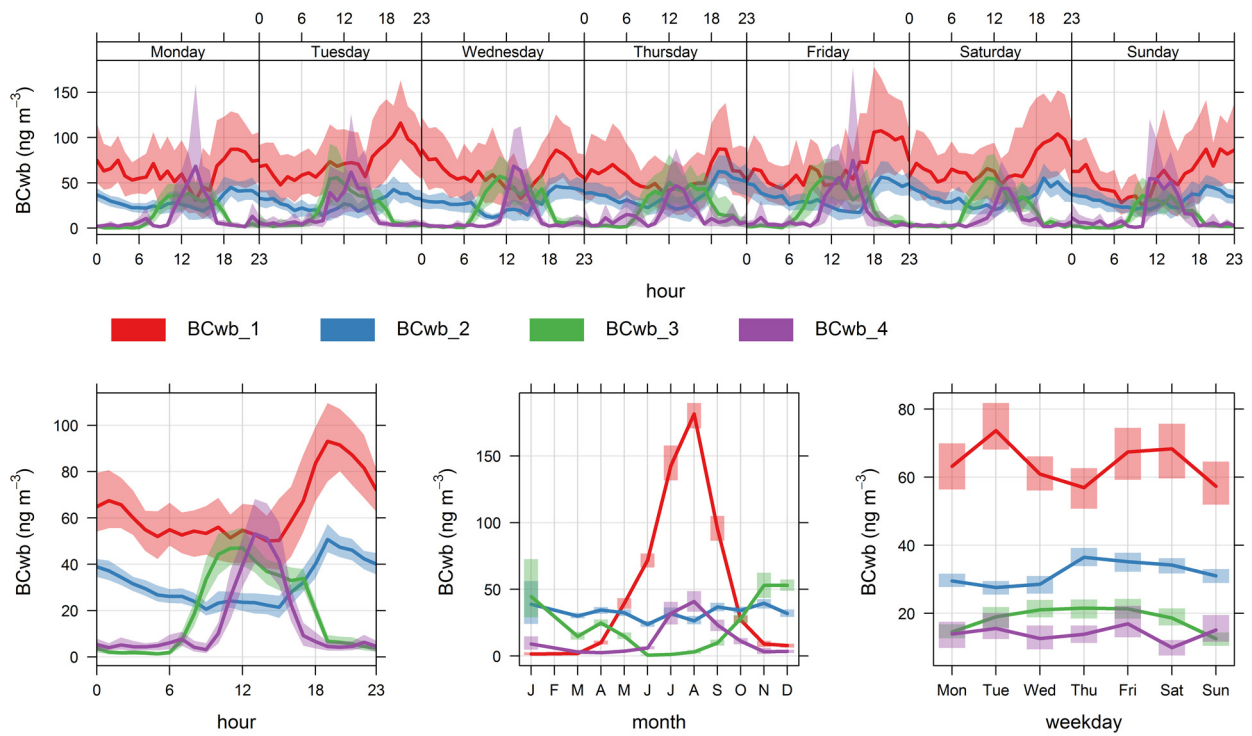


Figure 7. Time variability plot for the four fuzzy clusters' contributions to  $BC_{wb}$ .

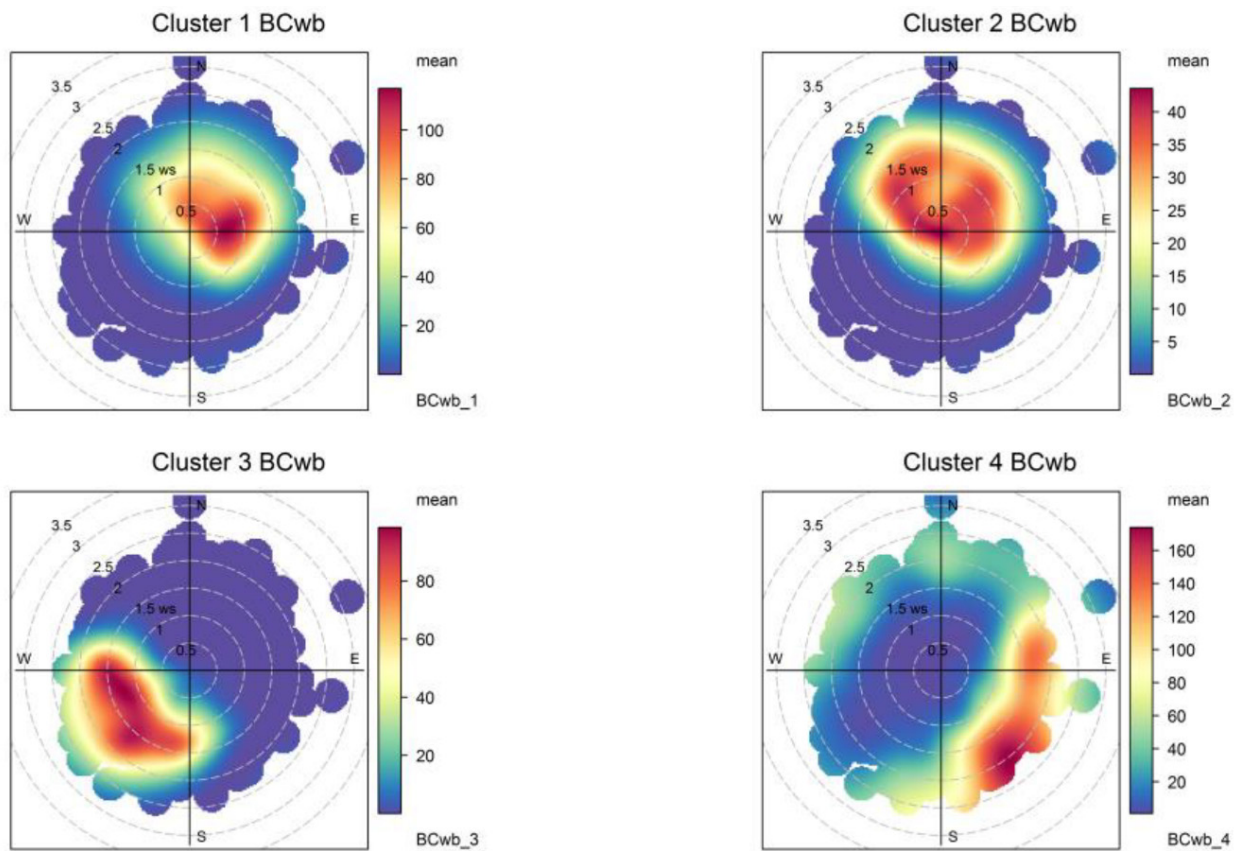


Figure 8. Bivariate plots for the four fuzzy clusters' contributions to  $BC_{wb}$ .

Clusters 1 and 2 have similar diel profiles with peaks in the evening hours but have different seasonality: cluster 1 contributions peak with ambient temperatures lower than 15 °C (Figure A6) and have a stronger seasonality, while cluster 2 contributions have no clear seasonality pattern and are associated to ambient temperatures above 10 °C (Figure A6). We identify these two clusters as local wood-burning sources; the combined contribution is 75% of total  $BC_{wb}$ .

Cluster 3 contributions rise in the afternoon and are zero overnight; they peak in the summer season, with high temperatures (Figure A6) and come from W-SW directions. Hence, this is Santiago's urban plume reaching the monitoring site, and this source contributes 14% of the total  $BC_{wb}$ .

Cluster 4 contributions come from S-SE directions and peak in winter around 1 pm, with no weekly seasonality. These contributions come under different synoptic conditions of low and high pressure (Figure A7); they likely come from residential cooking and heating and correspond to 11% of total  $BC_{wb}$ . In this regard, this noise cluster has a similar spatiotemporal pattern as the noise cluster found for  $BC_{ff}$ ; this means the residential sources S-SE of the monitoring site contributes to both BC fractions.

### 3.3. Source Apportionment of $BC_{ff}$ and $BC_{wb}$

The fuzzy clustering methodology (FUSTA) generates a source apportionment of BC at the monitoring site. The following figures show the daily contributions of the different sources resolved in this work; Appendix C presents results for hourly contributions.

Figures 9 and 10 show the daily source contributions for  $BC_{ff}$  and  $BC_{wb}$ , respectively. Local traffic contributions dominate  $BC_{ff}$ , and local wood-burning sources dominate  $BC_{wb}$ . Nonetheless, the noisy source contributions have the largest hourly spikes (Figures A8 and A9). Notice that the urban plume contributions are minimum in winter-time when the mixing layer over the city reaches minimum values [47], blocking air masses from arriving at the monitoring site. The urban plume contribution shows a rise towards the end of 2020, associated with less stringent lockdowns therein and a consequent increase in traffic activity levels [33].

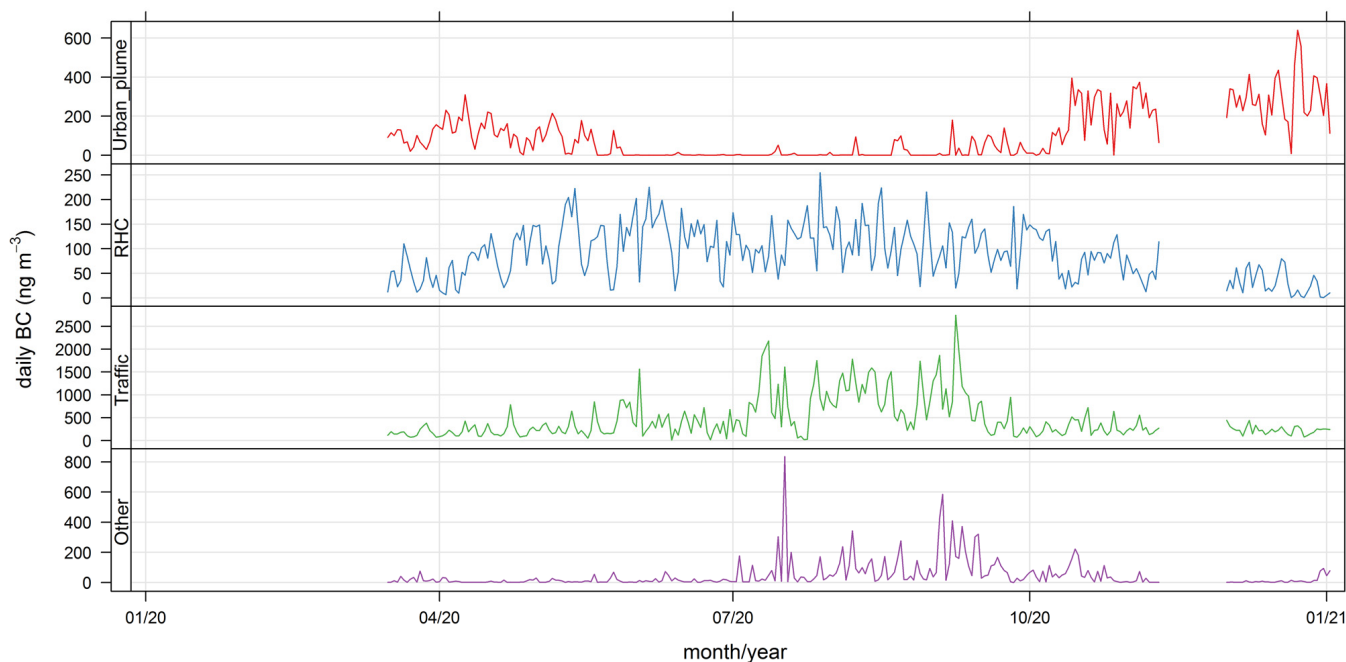
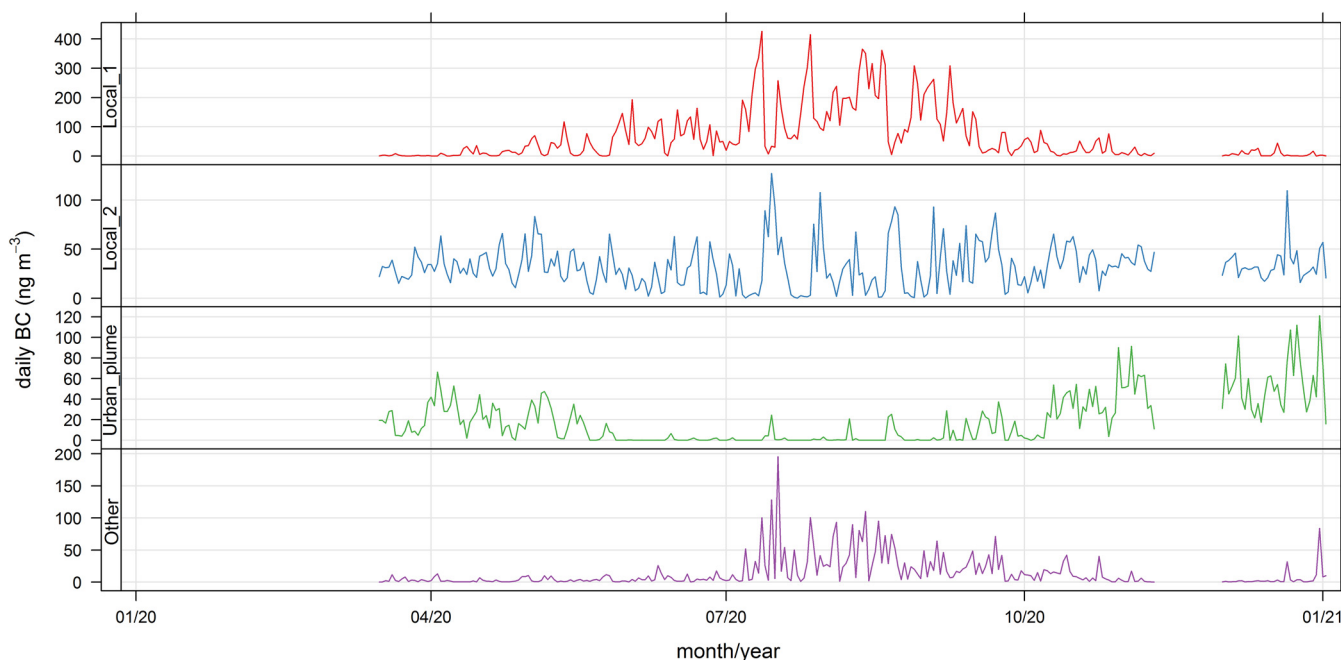


Figure 9. Time plot of daily source contributions to  $BC_{ff}$ .



**Figure 10.** Time plot of daily source contributions to  $BC_{wb}$ .

#### 4. Discussion

This is the first report of BC source apportionment conducted in Santiago, Chile that includes the effects of lockdowns brought on by the SARS-CoV-2 pandemics. Hence, the results reported here may be considered a baseline for future studies.

The total BC reductions associated with Santiago 2020 lockdowns—from 40% to 80%—are like the ones estimated for other cities worldwide: Delhi, India [25], up to 78%; Kigali, Rwanda [29], 59%; Sommerville, MA, USA [28], 22–56%; Wuhan, China [31], 39%. One limitation of our estimated reduction is that the baseline is not 2019 but 2015; since ambient  $PM_{2.5}$  has been steadily decreasing in Santiago for the period 2015–2020 [48], this means our estimates are upper bounds (in magnitude) of 2019–2020 BC reductions.

Regarding BC source apportionment during lockdown conditions,  $BC_{ff}$  is dominant all year long, between 82 and 86% of total BC in Santiago. This is higher than in other cities during lockdowns: 70% in Ahmedabad, India [30], 60–86% in Wuhan, China [31], 51–69% in Delhi, India [25], 50% in Kigali, Rwanda [29]. We ascribe this to the mild, Mediterranean climate of Santiago, the large fleet of motor vehicles therein and the lower proportion of wood-burning emissions as compared to the above cities.

The non-local contributions coming from the greater Santiago metropolitan area are associated with the development of anabatic winds during daylight hours, so these contributions are zero overnight; the spatial and temporal plots (Figures 5–8) show that FUSTA methodology separates this contribution from the local sources. This novel approach circumvents the use of an air quality model to estimate how much  $BC_{ff}$  (or  $BC_{wb}$ ) originates locally or is transported from upwind urban sources. In addition, the noisy fuzzy cluster concept handles intermittent sources arriving at the monitoring site, which are local emissions from residential cooking and heating; these are resolved from the other local sources because their spatiotemporal patterns are different. This split of local, non-local and intermittent contributions to ambient  $BC_{ff}$  and  $BC_{wb}$  concentrations will facilitate further air quality modeling studies for these ambient combustion tracer particles.

#### 5. Conclusions

A 2020 baseline of ambient  $BC_{ff}$  and  $BC_{wb}$  concentrations has been compiled for Santiago, Chile, during the SARS-CoV-2 lockdown periods, at an urban site located on the east border of the city.  $BC_{ff}$  is the dominant contribution all year long, accounting for

more than 80% of total BC. During the more restrictive lockdowns, total BC decreased by ~80% compared with a 2015 ambient BC campaign in the same part of the city; likewise, when lockdowns were relaxed, the decrease in total BC reached ~40% on the same comparison basis.

A new methodology to resolve local and non-local BC sources has been developed. This new methodology is based on a fuzzy clustering of ambient observations of BC and four meteorological variables: wind speed and direction, temperature, and pressure. This new methodology (named FUSTA) can resolve different spatiotemporal patterns (i.e., fuzzy clusters) of ambient BC, which arise from different BC sources contributing to ambient BC concentrations at the monitoring site. The methodology resolves, for instance, the arrival of Santiago's urban plume to the monitoring site due to the daylight anabatic wind regime in Santiago's basin. Besides, the methodology also handles intermittent sources like residential heating and cooking, especially in the winter season.

The application of FUSTA methodology to ambient  $BC_{ff}$  and  $BC_{wb}$  concentrations has led to the result that local sources are dominant in both BC fractions: traffic and wood burning sources, respectively, with 66% and 75%, respectively. The contributions from Santiago's urban plume arriving at the monitoring site increased towards the end of the year when lockdowns were relaxed; on average, this contribution reached 14% of  $BC_{ff}$  and  $BC_{wb}$  concentrations. Intermittent residential heating and cooking sources contribute to 7% and 11% of  $BC_{ff}$  and  $BC_{wb}$  concentrations, respectively. When these intermittent contributions are added to the regular spatiotemporal patterns (clusters), the total contribution of local residential heating and cooking sources reaches up to 20% and 86% for  $BC_{ff}$  and  $BC_{wb}$  concentrations, respectively.

**Supplementary Materials:** The following supporting information can be downloaded at: <https://www.mdpi.com/article/10.3390/ijerph192417064/s1>, Table S1: Database.csv, a database of ambient  $BC_{ff}$ ,  $BC_{wb}$ , and meteorological variables. Macro S1: R\_macros.zip, R-software macros to process data and make the fuzzy clustering and post-processing results.

**Author Contributions:** Conceptualization, H.J.; methodology, H.J. and C.A.; formal analysis, H.J., C.A. and A.M.V.; resources, H.J.; data curation, A.M.V.; writing—original draft preparation, H.J.; writing—review and editing, H.J. and A.M.V.; visualization, C.A. and A.M.V.; All authors have read and agreed to the published version of the manuscript.

**Funding:** This research was funded by ANID, grant number FONDAP 15110020 (CEDEUS), and Grant Fondecyt 1980894.

**Institutional Review Board Statement:** Not applicable.

**Informed Consent Statement:** Not applicable.

**Data Availability Statement:** Data are provided as Supplementary Files (see above).

**Acknowledgments:** Powered@NLHPC: This research was partially supported by the supercomputing infrastructure of the NLHPC (ECM-02). We acknowledge the comments and suggestions from three reviewers.

**Conflicts of Interest:** The authors declare no conflict of interest. The funders had no role in the design of the study; in the collection, analyses, or interpretation of data; in the writing of the manuscript; or in the decision to publish the results.

## Appendix A. Histogram of Absorption Ångström Exponents (AAE) and BC Source Apportionment

Figure A1 shows the histogram of all AAE values estimated using Equation (1) for the whole dataset of ambient measurements. The vertical lines stand for the 1st and 99th percentiles of estimated AAE values.

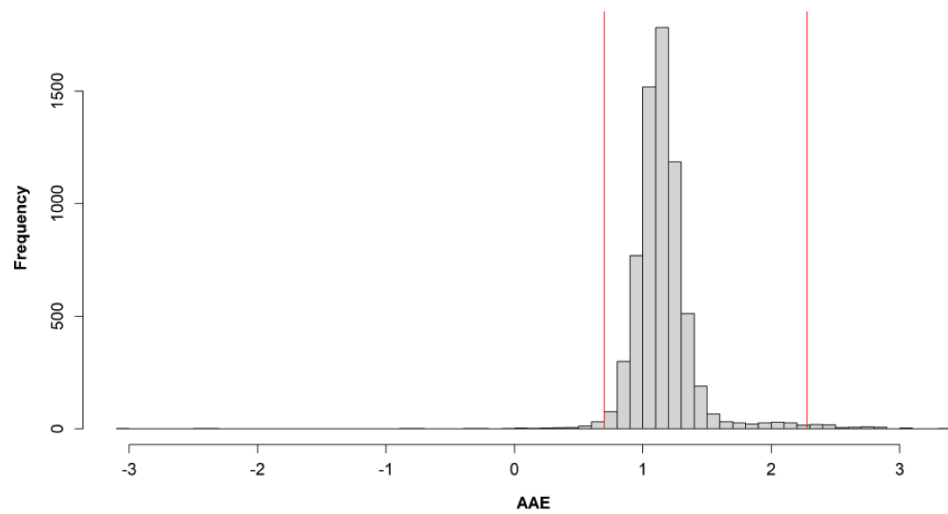


Figure A1. Histogram of AAE values computed using Equation (1).

From this analysis, it follows that the estimated AAE for fossil fuel and wood burning are:  $AAE_{ff} = 0.7$  and  $AAE_{wb} = 2.28$ , respectively. Using these exponents and applying Equations (2)–(5), the hourly estimates of  $BC_{ff}$  and  $BC_{wb}$  contributions are readily computed for the whole campaign. Figure A2 shows a time plot of those hourly estimates. There is a small number of negative values, which is caused by the extreme values in the above histogram of AAE; when daily averages are computed, no negative BC contributions occur, as shown below in Table A1.

Table A1. Statistical summary of daily average campaign results.

Statistic	AAE (-)	$BC_{ff}$ (ng/m <sup>3</sup> )	$BC_{wb}$ (ng/m <sup>3</sup> )	BC (ng/m <sup>3</sup> )
Minimum	0.888	92	20	112
1st quartile	1.073	383	70	470
Median	1.148	565	95	668
Mean	1.151	671	123	794
3rd quartile	1.228	807	150	972
Maximum	1.598	2938	522	3257

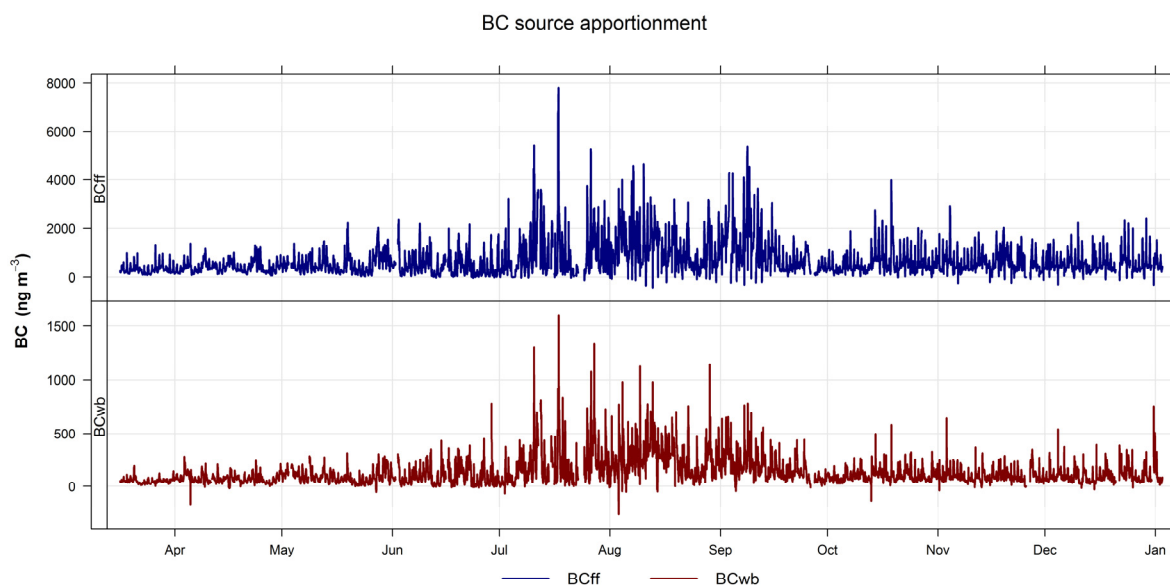


Figure A2. Time plot of hourly  $BC_{ff}$  and  $BC_{wb}$  concentrations, 2020 campaign.

To help visualize the time variability of  $BC_{wb}$  contributions, Figure A3 below shows only  $BC_{wb}$  at different time scales.

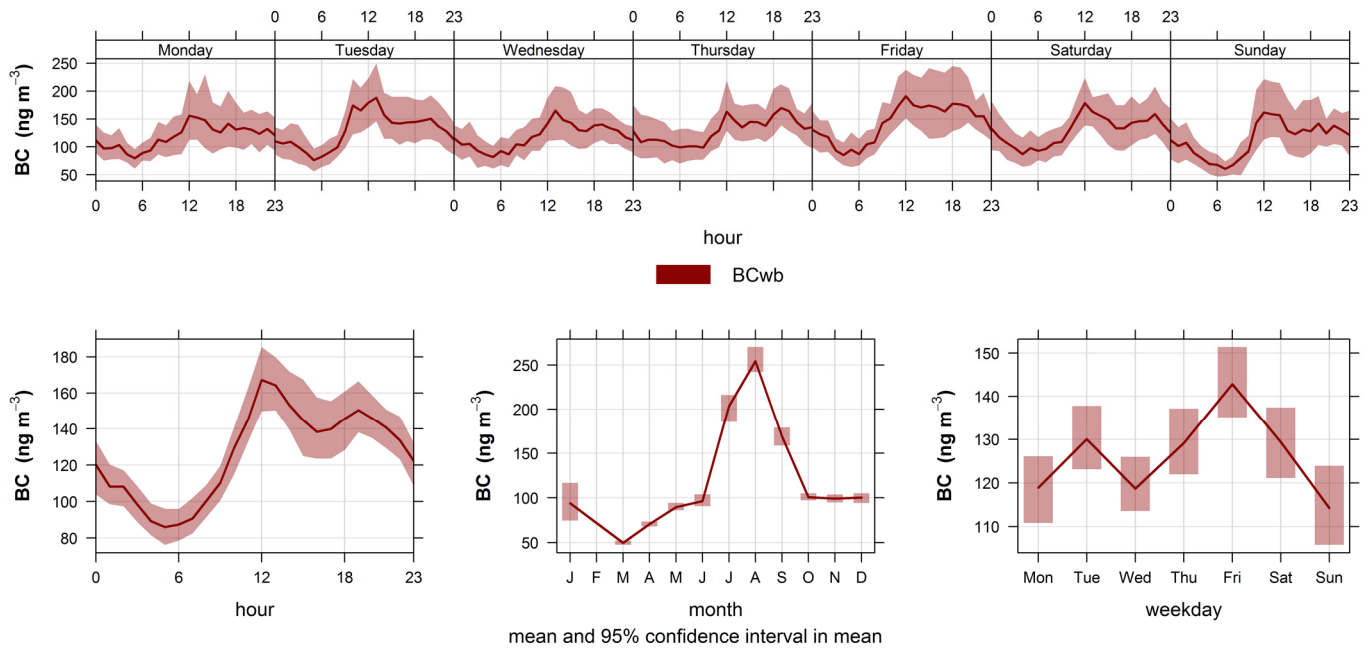


Figure A3. Time variability of  $BC_{wb}$  concentrations, 2020 campaign.

**Appendix B. Bivariate Plots for  $BC_{ff}$  and  $BC_{wb}$  Using Temperature and Pressure Instead of Wind Speed**

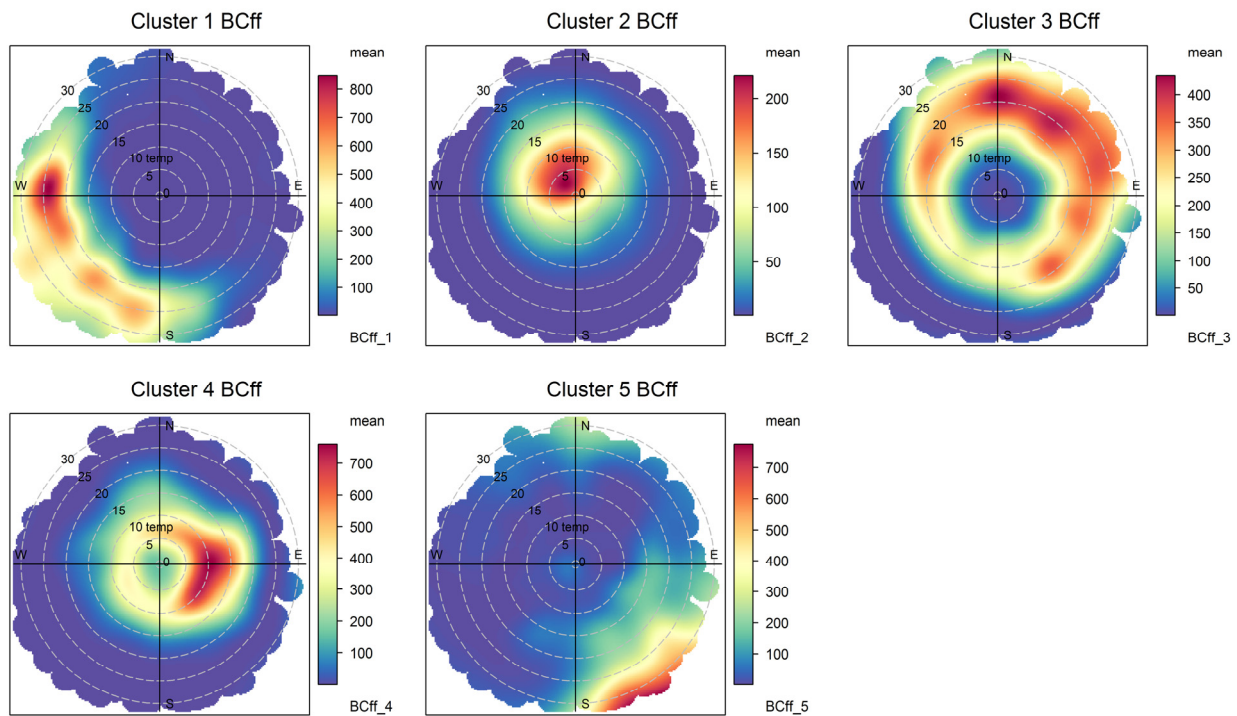


Figure A4. Bivariate plot of hourly  $BC_{ff}$  contributions, 2020 campaign, using temperature instead of wind speed.

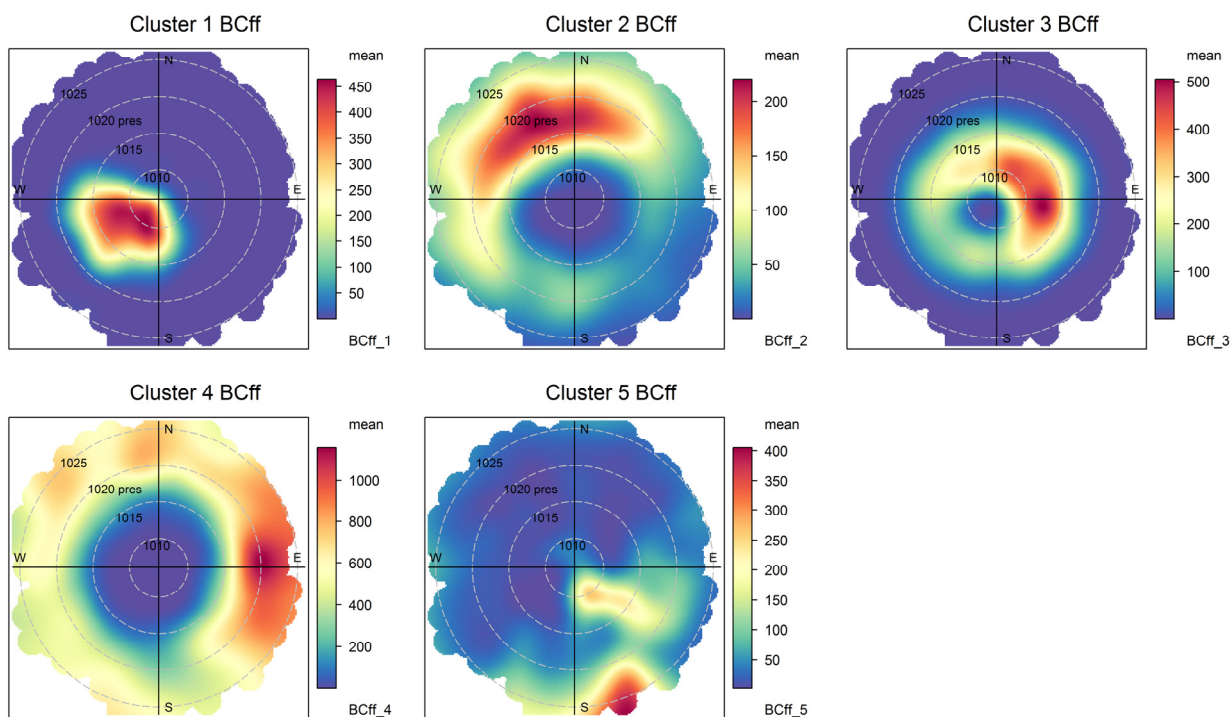


Figure A5. Bivariate plot of hourly  $BC_{ff}$  contributions, 2020 campaign, using pressure instead of wind speed.

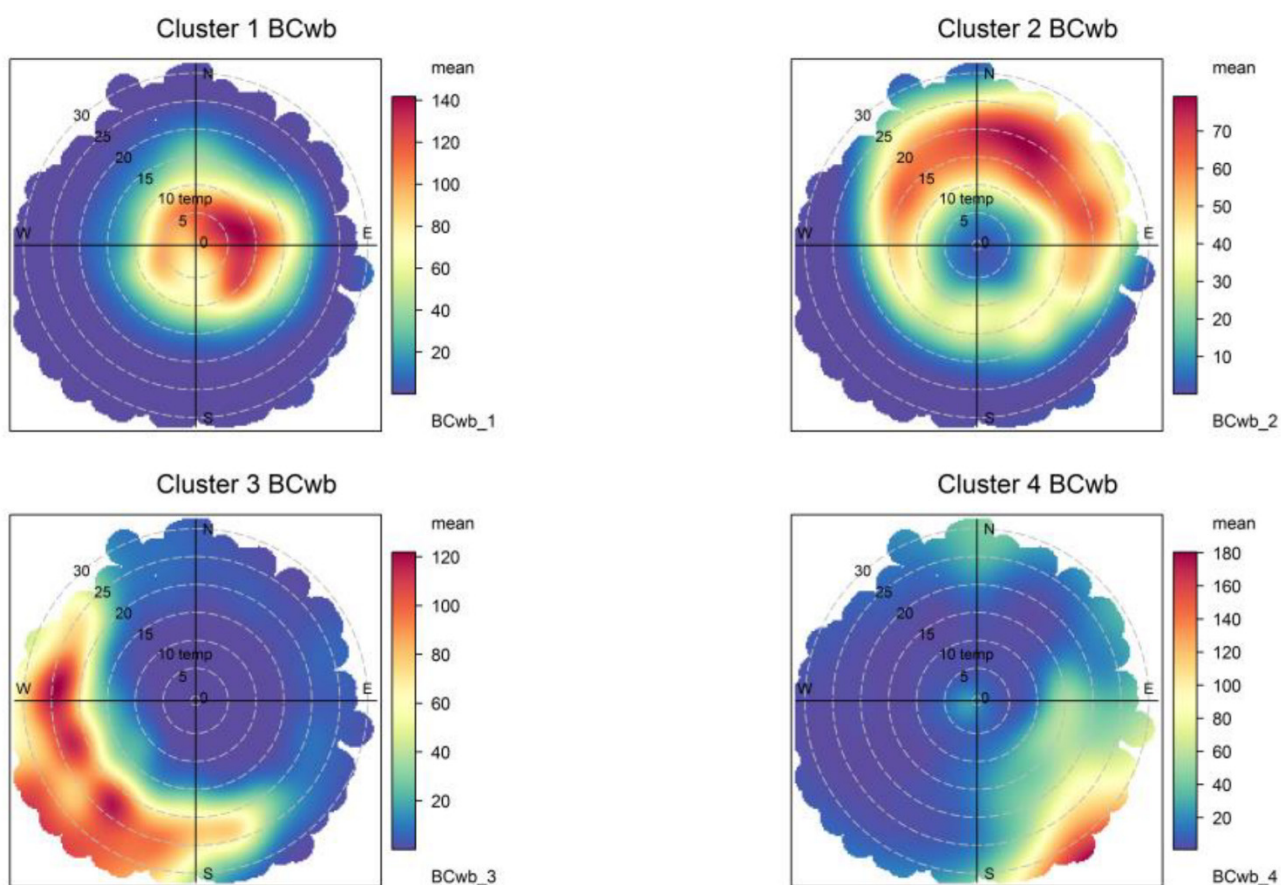


Figure A6. Bivariate plot of hourly  $BC_{wb}$  contributions, 2020 campaign, using temperature instead of wind speed.

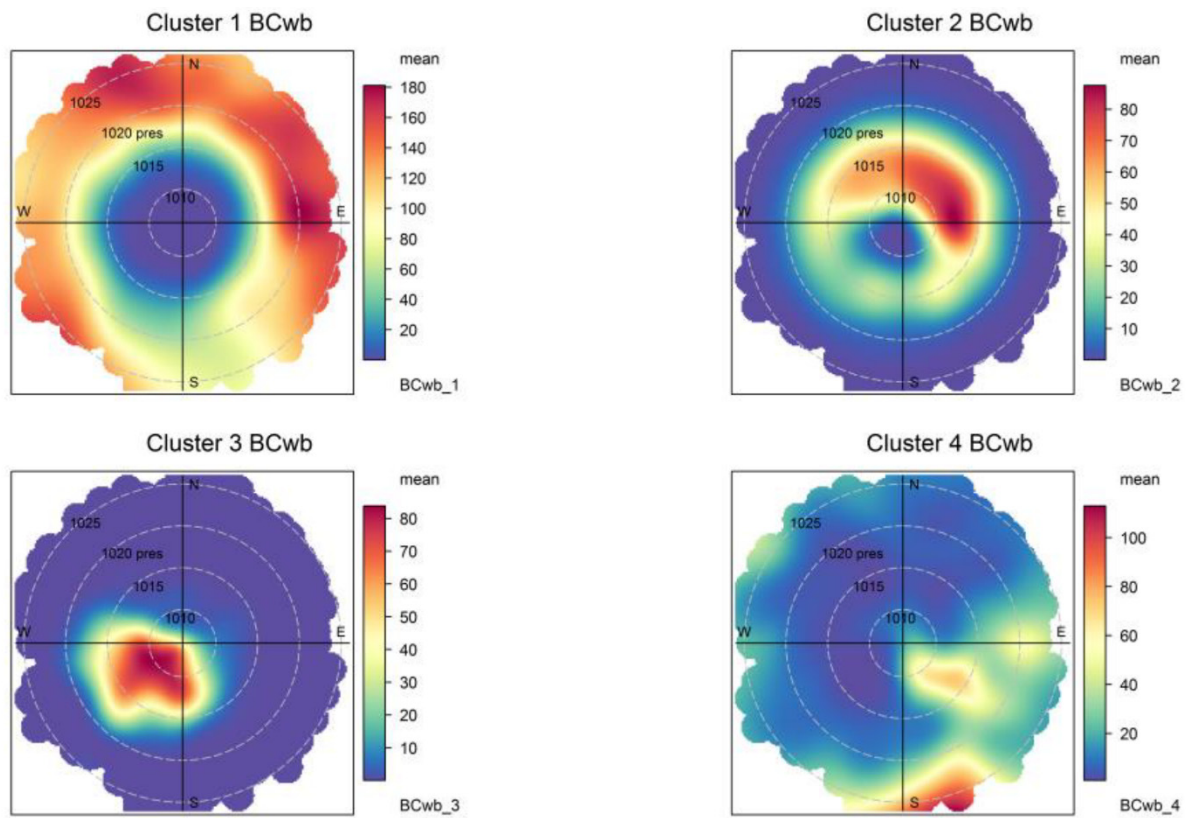


Figure A7. Bivariate plot of hourly  $BC_{wb}$  contributions, 2020 campaign, using pressure instead of wind speed.

Appendix C. Time Series Plots of Hourly Source Contributions to  $BC_{ff}$  and  $BC_{wb}$

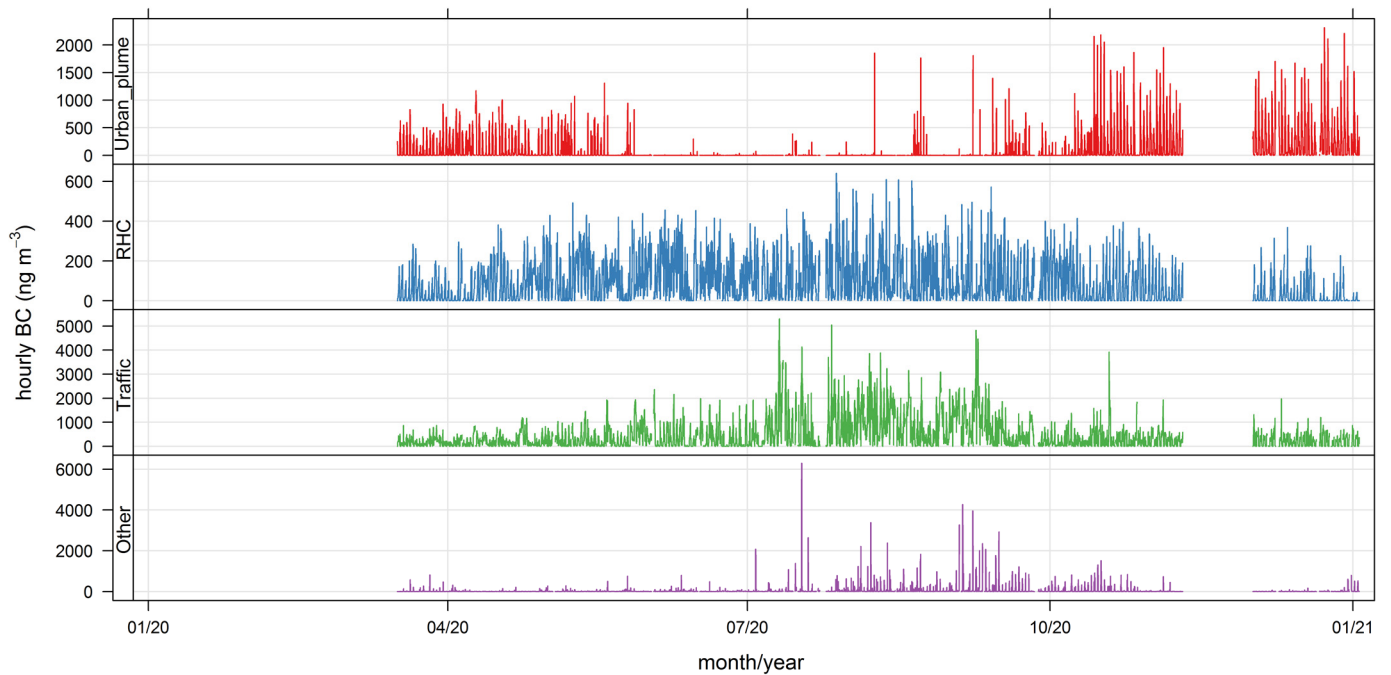
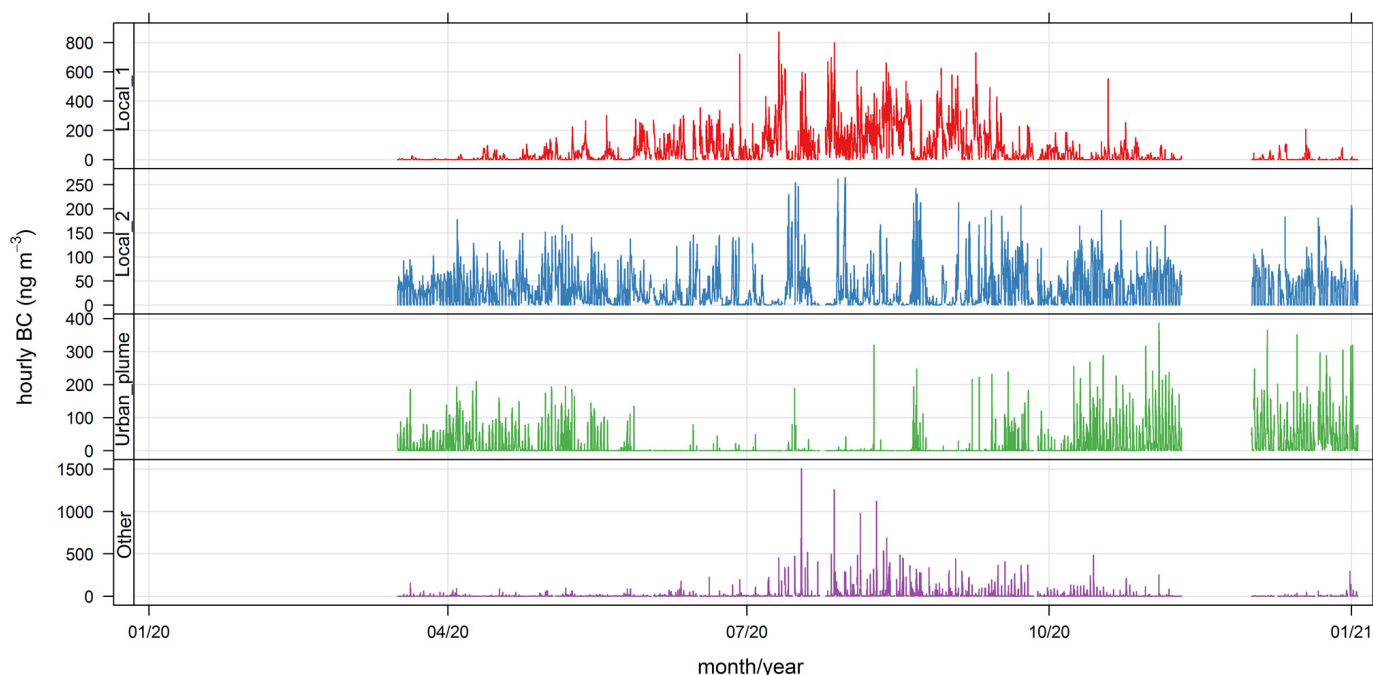


Figure A8. Time series plot of hourly  $BC_{ff}$  source contributions, 2020 campaign.



**Figure A9.** Time series plot of hourly  $BC_{wf}$  source contributions, 2020 campaign.

## References

- Hachem, M.; Loizeau, M.; Saleh, N.; Momas, I.; Bensefa-Colas, L. Short-term association of in-vehicle ultrafine particles and black carbon concentrations with respiratory health in Parisian taxi drivers. *Environ. Int.* **2021**, *147*, 106346. [[CrossRef](#)]
- Bista, S.; Fancello, G.; Chaix, B. Acute ambulatory blood pressure response to short-term black carbon exposure: The MobiliSense sensor-based study. *Sci. Total Environ.* **2022**, *846*, 157350. [[CrossRef](#)] [[PubMed](#)]
- Yang, J.; Sakhvidi, M.J.Z.; de Hoogh, K.; Vienneau, D.; Siemiatyck, J.; Zins, M.; Goldberg, M.; Chen, J.; Lequy, E.; Jacquemin, B. Long-term exposure to black carbon and mortality: A 28-year follow-up of the GAZEL cohort. *Environ. Int.* **2021**, *157*, 106805. [[CrossRef](#)]
- Shen, M.; Gu, X.; Li, S.; Yu, Y.; Zou, B.; Chen, X. Exposure to black carbon is associated with symptoms of depression: A retrospective cohort study in college students. *Environ. Int.* **2021**, *157*, 106870. [[CrossRef](#)]
- Suglia, S.F.; Gryparis, A.; Schwartz, J.; Wright, R.J. Association between Traffic-Related Black Carbon Exposure and Lung Function among Urban Women. *Environ. Health Perspect.* **2008**, *116*, 1333–1337. [[CrossRef](#)] [[PubMed](#)]
- Savouré, M.; Lequy, É.; Bousquet, J.; Chen, J.; de Hoogh, K.; Goldberg, M.; Vienneau, D.; Zins, M.; Nadif, R.; Jacquemin, B. Long-term exposures to PM<sub>2.5</sub>, black carbon and NO<sub>2</sub> and prevalence of current rhinitis in French adults: The Constances Cohort. *Environ. Int.* **2021**, *157*, 106839. [[CrossRef](#)] [[PubMed](#)]
- Ljungman, P.L.S.; Andersson, N.; Stockfelt, L.; Andersson, E.M.; Sommar, J.N.; Eneroth, K.; Gidhagen, L.; Johansson, C.; Lager, A.; Leander, K.; et al. Long-Term Exposure to Particulate Air Pollution, Black Carbon, and Their Source Components in Relation to Ischemic Heart Disease and Stroke. *Environ. Health Perspect.* **2019**, *127*, 107012. [[CrossRef](#)]
- World Health Organization. WHO Global Air Quality Guidelines: Particulate Matter (PM<sub>2.5</sub> and PM<sub>10</sub>), Ozone, Nitrogen Dioxide, Sulfur Dioxide and Carbon Monoxide. Available online: <https://www.who.int/publications/i/item/9789240034228> (accessed on 10 November 2022).
- Cavalli, F.; Viana, M.; Yttri, K.E.; Genberg, J.; Putaud, J.-P. Atmospheric Measurement Techniques Toward a Standardised Thermal-Optical Protocol for Measuring Atmospheric Organic and Elemental Carbon: The EUSAAR Protocol. *Atmos. Meas. Tech.* **2010**, *3*, 79–89. Available online: [www.atmos-meas-tech.net/3/79/2010/](http://www.atmos-meas-tech.net/3/79/2010/) (accessed on 10 November 2022). [[CrossRef](#)]
- Chow, J.C.; Watson, J.G.; Chen, L.-W.A.; Arnott, W.P.; Moosmüller, H.; Fung, K. Equivalence of Elemental Carbon by Thermal/Optical Reflectance and Transmittance with Different Temperature Protocols. *Environ. Sci. Technol.* **2004**, *38*, 4414–4422. [[CrossRef](#)]
- Petzold, A.; Ogren, J.A.; Fiebig, M.; Laj, P.; Li, S.-M.; Baltensperger, U.; Holzer-Popp, T.; Kinne, S.; Pappalardo, G.; Sugimoto, N.; et al. Recommendations for reporting “black carbon” measurements. *Atmos. Chem. Phys.* **2013**, *13*, 8365–8379. [[CrossRef](#)]
- Sandradewi, J.; Prévôt, A.S.H.; Szidat, S.; Perron, N.; Alfarra, M.R.; Lanz, V.A.; Weingartner, E.; Baltensperger, U. Using Aerosol Light Absorption Measurements for the Quantitative Determination of Wood Burning and Traffic Emission Contributions to Particulate Matter. *Environ. Sci. Technol.* **2008**, *42*, 3316–3323. [[CrossRef](#)] [[PubMed](#)]
- Mousavi, A.; Sowlat, M.H.; Hasheminassab, S.; Polidori, A.; Sioutas, C. Spatio-temporal trends and source apportionment of fossil fuel and biomass burning black carbon (BC) in the Los Angeles Basin. *Sci. Total Environ.* **2018**, *640–641*, 1231–1240. [[CrossRef](#)]

14. Healy, R.; Sofowote, U.; Su, Y.; Deboz, J.; Noble, M.; Jeong, C.-H.; Wang, J.M.; Hilker, N.; Evans, G.J.; Doerksen, G.; et al. Ambient measurements and source apportionment of fossil fuel and biomass burning black carbon in Ontario. *Atmos. Environ.* **2017**, *161*, 34–47. [[CrossRef](#)]
15. Küpper, M.; Quass, U.; John, A.C.; Kaminski, H.; Leinert, S.; Breuer, L.; Gladtko, D.; Weber, S.; Kuhlbusch, T.A.J. Contributions of carbonaceous particles from fossil emissions and biomass burning to PM<sub>10</sub> in the Ruhr area, Germany. *Atmos. Environ.* **2018**, *189*, 174–186. [[CrossRef](#)]
16. Liu, Y.; Yan, C.; Zheng, M. Source apportionment of black carbon during winter in Beijing. *Sci. Total. Environ.* **2018**, *618*, 531–541. [[CrossRef](#)] [[PubMed](#)]
17. Helin, A.; Niemi, J.V.; Virkkula, A.; Pirjola, L.; Teinilä, K.; Backman, J.; Aurela, M.; Saarikoski, S.; Rönkkö, T.; Asmi, E.; et al. Characteristics and source apportionment of black carbon in the Helsinki metropolitan area, Finland. *Atmos. Environ.* **2018**, *190*, 87–98. [[CrossRef](#)]
18. Mousavi, A.; Sowlat, M.H.; Lovett, C.; Rauber, M.; Szidat, S.; Boffi, R.; Borgini, A.; de Marco, C.; Ruprecht, A.A.; Sioutas, C. Source apportionment of black carbon (BC) from fossil fuel and biomass burning in metropolitan Milan, Italy. *Atmos. Environ.* **2019**, *203*, 252–261. [[CrossRef](#)]
19. Ambade, B.; Sankar, T.K.; Panicker, A.S.; Gautam, A.S.; Gautam, S. Characterization, seasonal variation, source apportionment and health risk assessment of black carbon over an urban region of East India. *Urban Clim.* **2021**, *38*, 100896. [[CrossRef](#)]
20. Xiao, S.; Yu, X.; Zhu, B.; Kumar, K.R.; Li, M.; Li, L. Characterization and source apportionment of black carbon aerosol in the Nanjing Jiangbei New Area based on two years of measurements from Aethalometer. *J. Aerosol Sci.* **2020**, *139*, 105461. [[CrossRef](#)]
21. Becerril-Valle, M.; Coz, E.; Prévôt, A.S.H.; Močnik, G.; Pandis, S.N.; Sánchez de la Campa, A.M.; Alastuey, A.; Díaz, E.; Pérez, R.M.; Artíñano, B. Characterization of atmospheric black carbon and co-pollutants in urban and rural areas of Spain. *Atmos. Environ.* **2017**, *169*, 36–53. [[CrossRef](#)]
22. Stampfer, O.; Austin, E.; Ganuelas, T.; Fiander, T.; Seto, E.; Karr, C.J. Use of low-cost PM monitors and a multi-wavelength aethalometer to characterize PM<sub>2.5</sub> in the Yakama Nation reservation. *Atmos. Environ.* **2020**, *224*, 117292. [[CrossRef](#)]
23. Herich, H.; Hueglin, C.; Buchmann, B. A 2.5 year's source apportionment study of black carbon from wood burning and fossil fuel combustion at urban and rural sites in Switzerland. *Atmos. Meas. Tech.* **2011**, *4*, 1409–1420. [[CrossRef](#)]
24. Gramsch, E.; Muñoz, A.; Langner, J.; Morales, L.; Soto, C.; Pérez, P.; Rubio, M.A. Black carbon transport between Santiago de Chile and glaciers in the Andes Mountains. *Atmos. Environ.* **2020**, *232*, 117546. [[CrossRef](#)]
25. Goel, V.; Hazarika, N.; Kumar, M.; Singh, V.; Thamban, N.M.; Tripathi, S.N. Variations in Black Carbon concentration and sources during COVID-19 lockdown in Delhi. *Chemosphere* **2021**, *270*, 129435. [[CrossRef](#)]
26. Dave, J.; Meena, R.; Singh, A.; Rastogi, N. Effect of COVID-19 lockdown on the concentration and composition of NR-PM<sub>2.5</sub> over Ahmedabad, a big city in western India. *Urban Clim.* **2021**, *37*, 100818. [[CrossRef](#)]
27. Sonbawne, S.M.; Devara, P.C.S.; Bhojar, P.D. Multisite characterization of concurrent black carbon and biomass burning around COVID-19 lockdown period. *Urban Clim.* **2021**, *39*, 100929. [[CrossRef](#)]
28. Hudda, N.; Simon, M.C.; Patton, A.P.; Durant, J.L. Reductions in traffic-related black carbon and ultrafine particle number concentrations in an urban neighborhood during the COVID-19 pandemic. *Sci. Total. Environ.* **2020**, *742*, 140931. [[CrossRef](#)]
29. Kalisa, E.; Adams, M. Population-scale COVID-19 curfew effects on urban black carbon concentrations and sources in Kigali, Rwanda. *Urban Clim.* **2022**, *46*, 101312. [[CrossRef](#)]
30. Rajesh, T.A.; Ramachandran, S. Assessment of the coronavirus disease 2019 (COVID-19) pandemic imposed lockdown and unlock effects on black carbon aerosol, its source apportionment, and aerosol radiative forcing over an urban city in India. *Atmos. Res.* **2021**, *267*, 105924. [[CrossRef](#)] [[PubMed](#)]
31. Wang, Q.; Wang, L.; Tao, M.; Chen, N.; Lei, Y.; Sun, Y.; Xin, J.; Li, T.; Zhou, J.; Liu, J.; et al. Exploring the variation of black and brown carbon during COVID-19 lockdown in megacity Wuhan and its surrounding cities, China. *Sci. Total Environ.* **2021**, *791*, 148226. [[CrossRef](#)] [[PubMed](#)]
32. Jorquera, H.; Villalobos, A.M. A new methodology for source apportionment of gaseous industrial emissions. *J. Hazard. Mater.* **2023**, *443*, 130335. [[CrossRef](#)]
33. ISCI. Urban Mobility Report for Santiago, under SARS-CoV-2 Pandemics. Available online: <https://isci.cl/wp-content/uploads/2021/06/Movilidad-RM-Reporte-ISCI-Entel-Ocean-Mayo-2021.pdf> (accessed on 27 October 2022).
34. Ministry of the Environment, Chile. National System of Air Quality Monitoring Information. Available online: <http://sinca.mma.gob.cl> (accessed on 5 April 2018).
35. Tobler, A.K.; Skiba, A.; Canonaco, F.; Mockik, G.; Rai, P.; Chen, G.; Bartyzel, J.; Zimnoch, M.; Styszko, K.; Nećki, J.; et al. Characterization and Source Apportionment of PM<sub>1</sub> Organic Aerosol in Krakow, Poland. *Atmos. Chem. Phys.* **2021**, *21*, 14893–14906. [[CrossRef](#)]
36. Jorquera, H.; Villalobos, A.M. Combining Cluster Analysis of Air Pollution and Meteorological Data with Receptor Model Results for Ambient PM<sub>2.5</sub> and PM<sub>10</sub>. *Int. J. Environ. Res. Public Health* **2020**, *17*, 8455. [[CrossRef](#)]
37. Bezdek, J.C.; Ehrlich, R.; Full, W. FCM: The fuzzy c-means clustering algorithm. *Comput. Geosci.* **1984**, *10*, 191–203. [[CrossRef](#)]
38. Uria-Tellaetxe, I.; Carslaw, D.C. Conditional bivariate probability function for source identification. *Environ. Model. Softw.* **2014**, *59*, 1–9. [[CrossRef](#)]
39. Ferraro, M.B.; Giordani, P. A toolbox for fuzzy clustering using the R programming language. *Fuzzy Sets Syst.* **2015**, *279*, 1–16. [[CrossRef](#)]

40. Ferraro, M.B.; Giordani, P.; Serafini, A. fclust: An R Package for Fuzzy Clustering. *R J.* **2019**, *11*, 198–210. [[CrossRef](#)]
41. Li, R.-P.; Mukaidono, M. Gaussian clustering method based on maximum-fuzzy-entropy interpretation. *Fuzzy Sets Syst.* **1999**, *102*, 253–258. [[CrossRef](#)]
42. Carslaw, D.C.; Beevers, S.D. Characterising and understanding emission sources using bivariate polar plots and k-means clustering. *Environ. Model. Softw.* **2013**, *40*, 325–329. [[CrossRef](#)]
43. Grange, S.K.; Lewis, A.C.; Carslaw, D.C. Source apportionment advances using polar plots of bivariate correlation and regression statistics. *Atmos. Environ.* **2016**, *145*, 128–134. [[CrossRef](#)]
44. Barraza, F.; Lambert, F.; Jorquera, H.; Villalobos, A.M.; Gallardo, L. Temporal evolution of main ambient PM<sub>2.5</sub> sources in Santiago, Chile, from 1998 to 2012. *Atmos. Chem. Phys.* **2017**, *17*, 10093–10107. [[CrossRef](#)]
45. Jorquera, H.; Barraza, F. Source apportionment of ambient PM<sub>2.5</sub> in Santiago, Chile: 1999 and 2004 results. *Sci. Total Environ.* **2012**, *435–436*, 418–429. [[CrossRef](#)] [[PubMed](#)]
46. Gramsch, E.; Cereceda-Balic, F.; Oyola, P.; Vonbaer, D. Examination of pollution trends in Santiago de Chile with cluster analysis of PM<sub>10</sub> and Ozone data. *Atmos. Environ.* **2006**, *40*, 5464–5475. [[CrossRef](#)]
47. Muñoz, R.C.; Undurraga, A.A. Daytime Mixed Layer over the Santiago Basin: Description of Two Years of Observations with a Lidar Ceilometer. *J. Appl. Meteorol. Climatol.* **2010**, *49*, 1728–1741. [[CrossRef](#)]
48. Jorquera, H. Air quality management in Chile: Effectiveness of PM<sub>2.5</sub> regulations. *Urban Clim.* **2021**, *35*, 100764. [[CrossRef](#)]